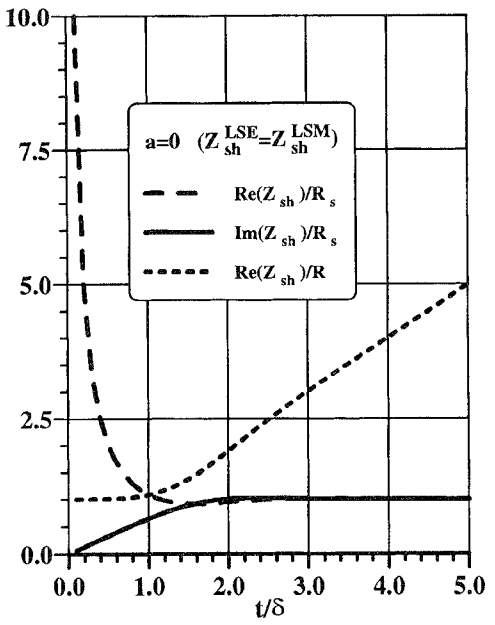

Fig. 5. Ratios of the real and imaginary parts of the sheet impedances to the real part of the surface impedance of thick conductors $R_s = 1/\sigma\delta$ and sheet resistance $R = 1/\sigma t$ as a function of t/δ for the LSE and LSM modes when $a = 0$. $\sigma = 5.88(10^7)$ S/m and F = 10 GHz.

It is also interesting to note that the sheet resistance and surface impedance are usually derived for a field distribution which depends only on the coordinate normal to the plane, i.e., only on y. In the present analysis, this corresponds to the specific case where $a = 0$. Indeed, only under these conditions, the two sheet impedances of the two modes are equal for all values of the thickness as shown in Fig. 5.

IV. Conclusion

This paper presents a detailed study of the concept of sheet impedance, defined as the ratio of the tangential electric field at the surface of a conductor to the conduction current per unit length it carries. We report that the sheet resistance depends on the field distribution in the structure. In the limit of thin conductors, the sheet impedance of a LSM mode is twice that of a LSE mode when the field varies slowly in the direction normal to the conductor ($a \to 1$). When the fields vary rapidly in the same direction, the sheet impedance of a LSE mode is twice that of a LSM mode when the conductor is very thin ($t/\delta \ll 1$). In the limit of thick conductors the sheet impedance approaches $(1 + j)/\sigma\delta$ and is independent of the field distribution.

References

[1] I. M. Pond, C. M. Krowne, and W. C. Carter, "On the application of complex resistive boundary conditions to model transmission lines consisting of very thin superconductors," *IEEE Trans. Microwave Theory Tech.*, vol. 37, no. 1, pp. 181–190, Jan. 1989.

[2] C. W. Kuo and T. Itoh, "A flexible approach combining the spectral domain method and impedance boundary condition for the analysis of microstrip line," *IEEE Microwave and Guided Wave Lett.*, vol. 1, pp. 172–174, July 1991.

[3] A. T. Shalaby, E. M. Zieur, and A. O. Attia, "Spectral domain analysis of high-T_c superconducting microstrip resonators," in *IEEE AP-S Int. Symp. Dig.*, 1993, pp. 193–196.

[4] J. C. Liou and K. M. Lau, "A solution to characteristics of planar transmission lines made of finite-thickness metal on multilayered media," in *IEEE MTT-S Int. Microwave Symp. Dig.*, 1990, pp. 179–181.

[5] Z. Cai and J. Bornemann, "Generalized spectral-domain analysis for multilayered complex media and high-T_c superconductor applications," *IEEE Trans. Microwave Theory Tech.*, vol. 40, pp. 2251–2257, Dec. 1992.

[6] S. Ramo, J. R. Whinnery, and T. Van Duzer, *Fields and Waves in Communication Electronics*. New York: Wiley, 1965, ch. 5.

[7] R. E. Matick, *Transmission Lines for Digital and Communication Networks*. New York: McGraw-Hill, 1969.

[8] E. C. Jordan and K. G. Balmain, *Electromagnetic Waves and Radiating Systems*. Englewood Cliffs: Prentice-Hall, 1968, pp. 153–158.

[9] D. Mirshekar-Syahkal, *Spectral Domain Method for Microwave Integrated Circuits*. New York: Wiley, 1990.

[10] T. Itoh, "Spectral domain immittance approach for dispersion characteristics of generalized printed transmission lines," *IEEE Trans. Microwave Theory Tech.*, vol. MTT-28, pp. 733–736, July 1980.

[11] C. M. Krowne, "Relationships for Green's function spectral dyadics involving anisotropic imperfect conductors imbedded in layered anisotropic media," *IEEE Antennas Propagat.*, vol. 37, pp. 1207–1211, Sept. 1989.

Accurate Analysis of Losses in Waveguide Structures by Compact Two-Dimensional FDTD Method Combined with Autoregressive Signal Analysis

Masafumi Fujii and Sumio Kobayashi

***Abstract*— An efficient two-dimensional finite-difference time-domain (2-D FDTD) method combined with an autoregressive (AR) signal analysis has been proposed for analyzing the propagation properties of microwave guiding structures. The method is especially suitable for analyzing lossy transmission lines; and in contrast with previous approaches, it is based on an algorithm of a real domain only. The algorithm is verified by comparing the numerical results with exact solutions for dielectric loaded rectangular waveguides. The conductor losses in a variety of microstrip lines and coplanar waveguides have been accurately estimated by solving the electromagnetic fields in the conductors directly.**

I. Introduction

This paper proposes a new algorithm based on two-dimensional finite-difference time-domain (2-D FDTD) method [1]–[3] combined with an autoregressive (AR) signal analysis [4] for predicting the conductor losses in microwave circuits such as in monolithic microwave/millimeter-wave integrated circuits (MMIC's) and multichip modules (MCM's). In previous 2-D FDTD methods [1], the waveguide structures are assumed to be uniform and infinitely long in the direction of wave propagation (say z), and support modes with propagation constants β independent of z. Those mean that the z derivative can be replaced with $j\beta$, and result in a formulation of the algorithm in complex domain. Recently new algorithm have been proposed for enabling 2-D FDTD analysis in real domain [2], [3], however, those are restricted in the analysis of loss-less lines.

In contrast with previous approaches, we assume that the waveguide has a finite length l, and is bounded with two infinitely large

Manuscript received August 31, 1995; revised February 15, 1996.

The authors are with the Sumitomo Metal Industries, Ltd., 1-8 Fuso-cho, Amagasaki, 660 Japan.

Publisher Item Identifier S 0018-9480(96)03793-3.

electric planes at both ends; in other words, we analyze an ideal resonator instead of an infinitely long transmission line. Under the assumption, the fields have a z dependency of $\cos(\beta z)$ or $\sin(\beta z)$ with $\beta = \pi/l$ (for the fundamental mode in z direction). Thus the 2-D FDTD analysis can be performed in real domain.

In this formulation, the fields excited by a pulse with a short time duration show generally a property of damped oscillation with a resonant frequency Ω and a damping factor ξ. The characteristic parameters of an infinitely long transmission line, the angular frequency ω and the attenuation coefficient α can be obtained from the damped oscillation parameters Ω and ξ with simple mathematical formula as described later. The situation is very analogous with the relations between the transmission line method and the resonance method in standard microwave impedance measurements [5].

An AR method is adopted in this paper to estimate the damped oscillation parameters Ω and ξ, because a damped oscillation satisfies exactly the autoregression equation. Although the AR signal analysis has been adopted to reduce the calculation time in FD-TD analyzes by predicting unknown future signals from the past time series [6], [7], the adoption of the AR method in this paper is for quite different purpose from the previous approaches.

Furthermore, the electromagnetic fields in conductors are directly analyzed by forming sufficiently small grids in the conductors compared to the skin depth. The number of grids are reduced by using graded grids, which are varied from submicron to millimeter to suppress numerical errors.

II. Mathematical Formulation

We suppose an inner region bounded by infinitely large electric planes at $z = 0$, and $z = l$, respectively. In this region, the electromagnetic fields can be expressed by

$$X(x, y, z) = \hat{X}(x, y) \sin(\beta z), \quad \text{for} \quad X = E_x, E_y, \quad \text{or} \quad H_z \tag{1}$$

and

$$Y(x, y, z) = \hat{Y}(x, y) \cos(\beta z), \quad \text{for} \quad Y = H_x, H_y, \quad \text{or} \quad E_z \tag{2}$$

where β is the phase constant given by π/l. Thus, the z derivatives of the fields X and Y can be replaced by β, and $-\beta$, respectively, and the electromagnetic fields are in real domain. Thus, Maxwell's curl equations can be written as follows:

$$\nabla_t \times \mathbf{E} + \nabla z \times \beta \mathbf{E}_t = -\mu_0 \frac{\partial \mathbf{H}}{\partial t} \tag{3}$$

and

$$\nabla_t \times \mathbf{H} - \nabla z \times \beta \mathbf{H}_t = \mathbf{J} + \sigma \mathbf{E} + \epsilon_0 \epsilon_r \frac{\partial \mathbf{E}}{\partial t} \tag{4}$$

where subscript t denotes the tangential components in x–y plane. Current source $\mathbf{J}$ in (4) is used for exciting the fields in the present algorithm; J_x or J_y component is used for the application in this paper. That is a raised cosine pulse given for J_y as an example by

$$J_y(x, y, z) = \begin{cases} \hat{J}_y(x, y) \sin^2\left(\frac{\pi t}{T}\right) \sin(\beta z), & \text{for} \quad 0 \le t \le T \\ 0, & \text{for} \quad T < t. \end{cases} \tag{5}$$

Maxwell's curl (3) and (4) are discretized in space on the basis of the compact FDTD grids as in [2].

The damped oscillation of the excited fields in the resonator can be written by the following equation for a multimode case

$$f_n = \sum_{k=1}^{K} [\exp(-\xi_k n \Delta t_s)\{A_{fk} \cos(\Omega_k n \Delta t_s) + B_{fk} \sin(\Omega_k n \Delta t_s)\}], \quad \text{for} \quad n = 1, 2, \cdots \tag{6}$$

where f_n denotes a field component at nth sampling period $n\,\Delta t_s$, and K the total number of modes. The field component in (6) rigorously satisfies an autoregressive equation

$$\sum_{k=0}^{2K} a_k f_{n-k} = 0, \quad \text{with} \quad a_0 = 1, \quad \text{for} \quad n = 2K + 1, 2K + 2, \cdots. \tag{7}$$

This is easily shown by using the z-transform. The z-transform of (6) is given by

$$F(Z) = \frac{P_K(Z)}{Q_K(Z)} \tag{8}$$

with

$$Q_K(Z) = \prod_{k=1}^{K} \{Z^2 - 2Z \exp(-\xi_k \Delta t_s) \cos(\Omega_k \Delta t_s) + \exp(-2\xi_k \Delta t_s)\} \tag{9}$$

where $P_K(Z)$ is a polynomial of Z with $2K$ order at most. Equation (9) can be rewritten as

$$Q_K(Z) = \sum_{k=0}^{2K} a_k Z^{2K-k}, \quad \text{with} \quad a_0 = 1. \tag{10}$$

On the other hand, the z-transform $F(Z)$ has a property of

$$F(Z) = \sum_{n=0}^{\infty} f_n Z^{-n}. \tag{11}$$

By combining (8) and (11), we can get the autoregressive equation (7).

AR method is applied to the time series data which are later than the time $T + 2K\,\Delta t_s$, where T is the duration of the exciting pulse. After determining the autoregression parameters a_n with the AR method, the parameters of the damped oscillation Ω_k and ξ_k can be obtained by solving

$$Q_K(Z) = 0 \tag{12}$$

because the roots of (12) are given by

$$Z_k = \exp(-\xi_k \Delta t_s \pm j\Omega_k \Delta t_s), \quad \text{for} \quad k = 1, 2, \cdots, K. \tag{13}$$

The angular frequency ω_k and attenuation constant α_k for a given phase constant β in an infinitely long transmission line have the following relations to the damped oscillation parameters of the transmission line resonator Ω_k and ξ_k,

$$\omega_k = (\Omega_k^2 + \xi_k^2)^{1/2} \tag{14}$$

and

$$\alpha_k = \frac{\xi_k}{\frac{d\omega_k}{d\beta_k}}. \tag{15}$$

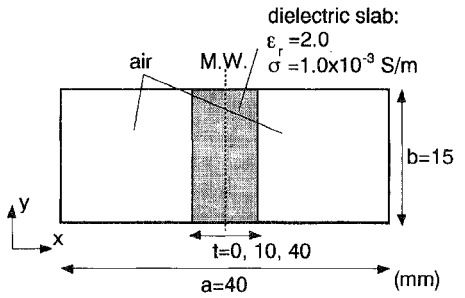

Fig. 1. The cross section of the dielectric loaded rectangular waveguide. Three cases were analyzed: i) air-filled waveguide ($t = 0$ mm), ii) waveguide with centered dielectric slab ($t = 10$ mm), and iii) dielectric-filled waveguide ($t = 40$ mm). The grid size adopted in cases i) and iii) is 0.9524×0.9375 mm. And that in case ii) is 1.0×0.9375 mm in the dielectric region and 0.9375×0.9375 mm in the air region. A magnetic wall condition is set on the vertical center of the waveguides.

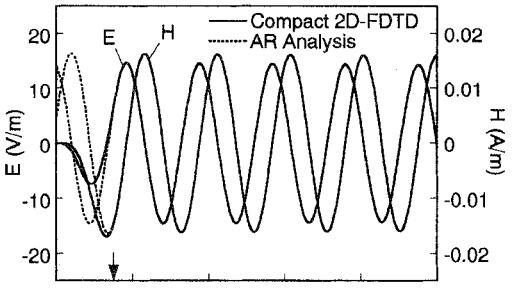

(a)

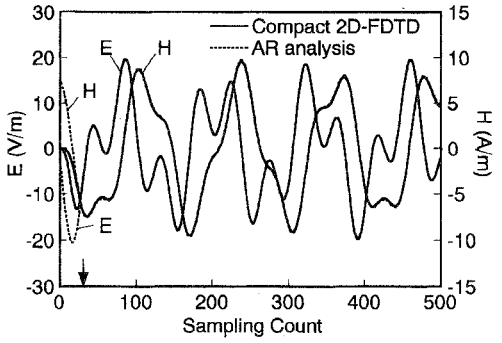

(b)

Fig. 2. The time series FDTD signals of the electric and magnetic fields at the center of the rectangular waveguide and the fitting results by the AR signal analysis ($\beta = 40$ rad/m). (a) The single TE_{10} mode in the rectangular waveguide with centered dielectric slab. The estimated frequency and attenuation constant by the AR method are 3.44 GHz and 1.47 dB/m, respectively. (b) The multimode of TE_{10} and TE_{30} modes in the dielectric-filled rectangular waveguide. The estimated frequencies and attenuation constants are 2.97 GHz and 2.55 dB/m for TE_{10} mode, and 7.80 GHz and 6.86 dB/m for TE_{30} mode, respectively. The AR method is applied after the time pointed by the downward arrows.

III. Results and Discussion

A. Dielectric Loaded Rectangular Waveguide

The present method was applied to the analysis of dielectric loaded rectangular waveguides. Three cases were analyzed as shown in Fig. 1: i) air-filled waveguide, ii) waveguide with centered dielectric slab with its width $t = 10$ mm, and iii) dielectric-filled waveguide with $t = 40$ mm.

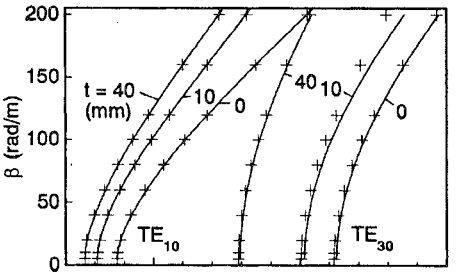

(a)

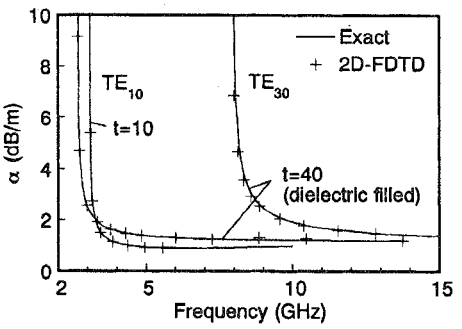

(b)

Fig. 3. The 2-D FDTD results of (a) the phase constants and (b) the attenuation constants compared with the exact solutions [8] of the dielectric loaded rectangular waveguides shown in Fig. 1.

The dimensions of the waveguide are 40 mm in width a, 15 mm in height b. The dielectric constant ϵ_r and the conductivity σ of the dielectric material were set to be 2.0 and 1.0×10^{-3} S/m respectively. The waveguide wall was assumed to be a perfect conductor, and the magnetic wall condition is set on the vertical center of the waveguide. The adopted grid size was around 1 mm square. The distribution of exciting pulse was a sum of TE_{10} and TE_{30} mode for the cases i) and iii), and TE_{10} mode for case ii). The pulse duration T was set to be a half cycle of the resonant oscillation for air-filled case. The parameter K for AR analysis was chosen to be two for all cases.

Fig. 2 shows the time series voltage and current in the waveguides calculated for $b = 40$ rad/m; Fig. 2(a) is for case ii), and Fig. 2(b) for case iii). The time series data in Fig. 2(a) and (b) demonstrate single and double mode damping oscillation respectively after the end of the launched raised cosine pulse. The fitting results by the AR signal analysis show excellent agreements with FDTD data.

The dispersion characteristics of α and β, shown in Fig. 3 are in good agreement with the exact solutions in [8]. These results show the validity of the present algorithm combined with the AR method.

B. Microstrip Lines

Three types of microstrip lines are investigated: a narrow copper-polyimide significantly lossy line for MCM applications, a wide silver-alumina slightly lossy line, and microstrip lines fabricated on a GaAs substrates with a passivation film for MMIC applications [9], [10].

1) Copper-Polyimide Microstrip Line: The cross section of the line is shown in Fig. 4. The materials are copper for conductors and polyimide for dielectric. The strip conductor width and thickness are 25 μm and 4 μm, respectively. The dielectric thickness is 8 μm.

The magnetic wall condition is set on the vertical center of the strip conductor. The electrical wall conditions are set on the top and bottom boundaries, and the magnetic wall condition is set on the outer side boundary due to convenience for grid formation. The absorbing

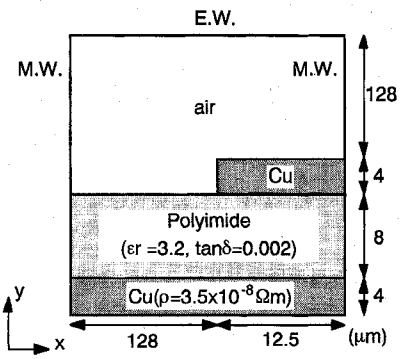

Fig. 4. The cross section of the copper-polyimide microstrip line. In the analysis, electric wall conditions are set on the top and bottom boundaries and magnetic wall conditions are set on the side and the vertical center boundaries.

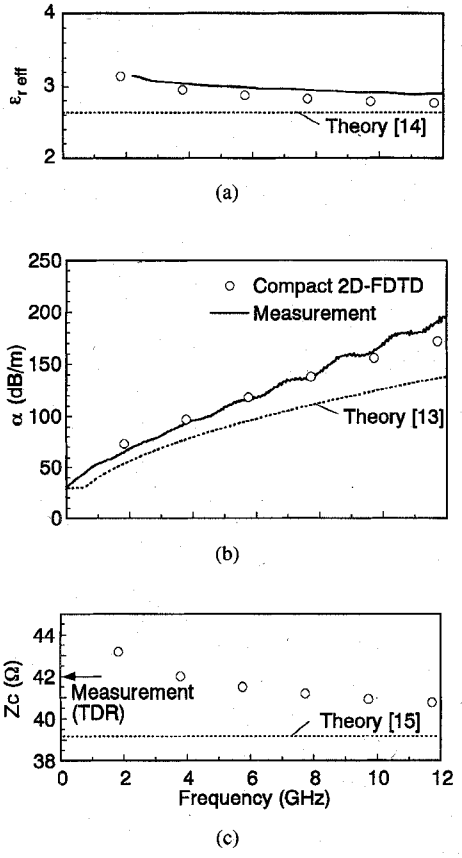

Fig. 5. The comparison of the computational results together with the conventional theoretical results and experimental data for the copper-polyimide microstrip line.

boundary conditions (ABC's) are not adopted here, because the outer side and top boundaries are placed far away from the strip conductor, so they do not affect the calculated results. A series of preliminary calculation showed that the effects of analytical region are negligible for parameter estimation when the width (x-direction) and the height (y-direction) of the region are larger than ten times of the dielectric thickness. Therefore the width and the height of the analytical region were chosen to be 16 times of the dielectric thickness, respectively.

In the graded grids formation, hyperbolic sine function [11] is adopted in the outer region, and hyperbolic tangent function [11] is adopted in the inner regions. It is known that these types of grid formation generate the gradually changed grid spacings, and minimize

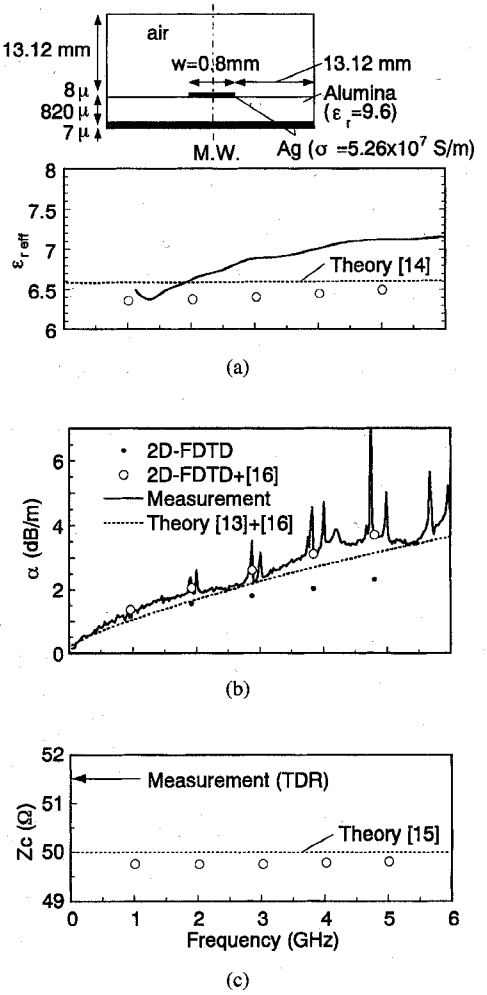

Fig. 6. The computational results of the silver-alumina microstrip line. The effect of the surface roughness was considered with the empirical formula [16] both for computational and theoretical results.

the numerical error [12]. The minimum grid spacing is chosen to be a tenth of the skin depth. These criteria for grid generation are adopted throughout the analysis described below.

The computational results of the effective dielectric constant, attenuation constant, and characteristic impedances are compared together with the experimental and the conventional theoretical results [13] in Fig. 5. The sample is measured with network analyzer HP8510 and microwave probes (Cascade Microtech Inc.). The characteristic impedance measured with time domain reflectometry (TDR) was 42 Ω. Ripples in the measured attenuation constant in Fig. 5, which is due to the impedance mismatch, are suppressed by the large insertion loss of the sample. The computational results agree well with the measured data.

In contrast with the computational results, the conventional TEM mode approximation theory fails to predict the attenuation constant. In addition, the conventional theories [14], [15], which assume TEM mode propagation, also fail to predict the frequency dispersion properties of effective dielectric constant and characteristic impedance observed in a lossy transmission line.

2) Silver-Alumina Microstrip Line: The slightly lossy microstrip line of 0.8 mm wide silver strip conductor ($\sigma = 5.26 \times 10^7$ S/m) and 0.82 mm thick 96% pure alumina substrate ($\epsilon_r = 9.6$) as shown in the inset of Fig. 6 was investigated. The alumina substrate has a surface roughness of approximately 1 μm. The sample was measured

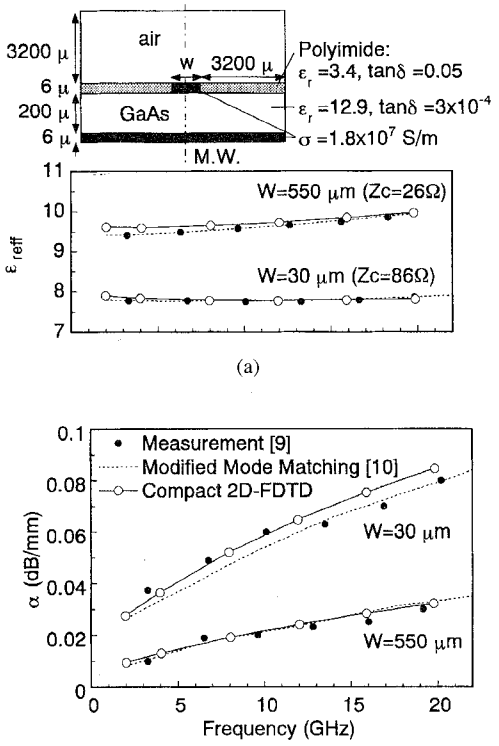

Fig. 7. The computational results of the microstrip lines fabricated on a GaAs substrates compared with the published data [9], [10].

with a network analyzer and microstrip-coaxial transform launchers. The measured characteristic impedances was 51.5 Ω. The sharp peaks in the measured attenuation constant in Fig. 6 were produced by the unnecessary resonances between the launchers due to the reflection at the connection of the sample and the launchers.

The grids are also formed by hyperbolic sine or hyperbolic tangent function. The computational results of the effective dielectric constants, attenuation constants, and characteristic impedances are compared with the conventional theoretical results and measured results in Fig. 6. The effects of surface roughness were considered with the empirical formula [16] both for computational and theoretical results. The attenuation constants obtained with the three approaches show satisfactory agreement with each other.

3) Microstrip Lines Fabricated on GaAs Substrates: The microstrip configurations analyzed is shown in Fig. 7. The strip line widths are 550 μm and 30 μm, and the thickness of the conductor and the GaAs substrate is 6 μm and 200 μm, respectively. The conductance of the conductors is 1.8×10^7 S/m, and the dielectric constant ϵ_r and the loss tangent $\tan\delta$ are 12.9 and 3×10^{-4} for the GaAs substrate, and 3.4 and 5×10^{-2} for the polyimide passivation film, respectively. The results were compared with precise measurement with a ring resonator method [9] and numerical results with a mode matching technique [10]. The grids are also formed by hyperbolic sine and hyperbolic tangent function. The characteristic impedance is 26 Ω for 550 μm wide line and 86 Ω for 30 μm wide line. The 2-D FDTD results show good agreement with the published data.

C. Coplanar Waveguide

The cross section of the coplanar waveguide under investigation is shown in the inset of Fig. 8. The materials are gold ($\sigma = 3.0 \times 10^7$ S/m) for the conductors and 99.9% pure sapphire ($\epsilon_r = 9.9$) for the dielectric substrate. The characteristic impedance measured with TDR was 50 Ω. In the analysis, the hyperbolic sine and hyperbolic tangent types of graded grids are also adopted, and electric and magnetic wall conditions are set as in the microstrip configuration. The analytical region of the coplanar waveguide of the line width w and the gap s is chosen to be $16(w/2 + s)$, from the preliminary analysis on the influence of the boundaries. The S-parameters were directly measured up to 40 GHz with a network analyzer and microwave probe. The characteristic impedance of the sample is well controlled to be 50 Ω.

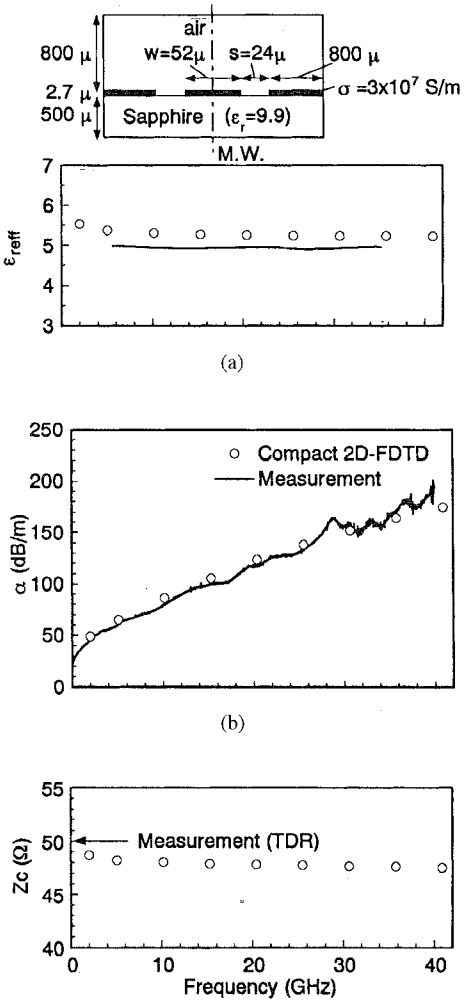

Fig. 8. The computational results of the coplanar waveguide together with experimental data.

The numerical and experimental results for the attenuation constants, effective dielectric constants, and characteristic impedances are shown in Fig. 8. The numerical results both for the attenuation constants and the frequency dispersion of the effective dielectric constants are in satisfactory agreement with the experimental data.

IV. Conclusion

A compact 2-D FDTD algorithm formulated in real domain is proposed. The 2-D FDTD method combined with an AR signal analysis method is applied to the analysis of propagation properties of waveguiding structures. The present algorithm is validated by comparing the computational results with the exact solutions for dielectric loaded rectangular waveguides. The conductor losses in various types of microstrip lines and a coplanar waveguide are ana-

lyzed. The electromagnetic fields in conductors are directly analyzed by forming sufficiently small grids compared to the skin depth, and accurate attenuation constants are obtained for the lossy structures.

ACKNOWLEDGMENT

The authors would like to acknowledge Mr. Sakamoto for his help in the computational experiments, and to the members of the Design Group for their continuous encouragements.

REFERENCES

[1] V. J. Brankovic, D. V. Krupezevic, and F. Arndt, "An efficient two-dimensional graded mesh finite-difference time-domain algorithm for shielded or open waveguide structures," *IEEE Trans. Microwave Theory Tech.*, vol. 40, pp. 2272–2277, Dec. 1992.

[2] A. C. Cangellaris, "Numerical stability and numerical dispersion of a compact 2-D/FDTD method used for dispersion analysis of waveguides," *IEEE Microwave Guided Wave Lett.*, vol. 3, no. 1, pp. 3–5, Jan. 1993.

[3] S. Xiao and R. Vahldieck, "An improved 2-D FDTD algorithm for hybrid modes analysis of quasiplanar transmission lines," in *IEEE MTT-S Int. Microwave Symp. Dig.*, Atlanta, June 1993, pp. 421–424.

[4] S. M. Kay and S. L. Marple, "Spectrum analysis—A modern perspective," *Proc. IEEE*, vol. 69, pp. 1380–1419, 1981.

[5] R. K. Hoffmann, *Handbook of Microwave Integrated Circuits.* Boston: Artech House, 1987, pp. 205.

[6] W. L. Ko and R. Mittra, "A combination of FD-TD and Prony's method for analyzing microwave integrated circuits," *IEEE Trans. Microwave Theory Tech.*, vol. 39, pp. 2176–2181, 1991.

[7] J. Chen, C. Wu, K. Wu, and J. Litva, "Combining an autoregressive (AR) model with the FD-TD algorithm for improved computational efficiency," in *IEEE MTT-S Int. Microwave Symp. Dig.*, Atlanta, June 1993, pp. 749–752.

[8] R. E. Collin, *Field Theory of Guided Waves*, 2nd ed. New York: IEEE Press, 1991, pp. 411.

[9] H. Finlay, R. H. Jansen, J. A. Jenkins, and I. G. Eddison, "Accurate characterization and modeling of transmission lines for GaAs MMIC's," *IEEE Trans. Microwave Theory Tech.*, vol. 36, pp. 961–967, June 1988.

[10] W. Heinrich, "Full-wave analysis of conductor losses on MMIC transmission lines," *IEEE Trans. Microwave Theory Tech.*, vol. 38, pp. 1468–1472, Oct. 1990.

[11] J. F. Thompson, Z. U. A. Warsi, and C. W. Mastin, *Numerical Grid Generation.* New York: North-Holland, 1985, pp. 305–310.

[12] ——, pp. 171–187.

[13] R. A. Pucel, D. J. Masse, and C. P. Hartwig, "Losses in microstrip," *IEEE Trans. Microwave Theory Tech.*, vol. MTT-16, pp. 342–350, June 1968.

[14] M. Krishning and R. H. Jansen, "Accurate model for effective dielectric constant of microstrip with validity up to millimeter-wave frequencies," *Electron. Lett.*, vol. 18, pp. 272–273, 1982.

[15] P. Pramanic, and P. Bhartia, "Computer-aided design models for millimeter-wave finlines and suspended-substrate microstrip lines," *IEEE Trans. Microwave Theory Tech.*, vol. MTT-33, pp. 1429–1435, 1985.

[16] D. Hollmann, S. Haffa, F. Rostan, and W. Wiesbeck, "The introduction of surface resistance in the three-dimensional finite-difference method in frequency domain," *IEEE Trans. Microwave Theory Tech.*, vol. 41, pp. 893–895, 1993.

A Simple Formula for the Concentration of Charge on a Three-Dimensional Corner of a Conductor

Yimin Zhang and A. H. Zemanian

***Abstract*—A major problem in the computation of capacitance coefficients for microwave transmission and VLSI interconnection systems is caused by the singularities in the electric field at the corners and edges of conductors. For edges, a solution is given by the Duncan correction, which is based on a two-dimensional (2-D) polar expansion of the field. No such exact expansion exists for corners. Recent research by Beagles and Whiteman has yielded an asymptotic expansion for the electric field in the vicinity of a rectangular three-dimensional conductive corner, and this is used to derive a simple formula for the charge Q (in coulombs) concentrated at any such corner. The formula is $Q = 1.307\,\varepsilon d(V_c - V_s)$, where ε is the dielectric permittivity (in farads per meter) of the medium surrounding the conductive corner, d is the length (in meters) of one side of a cubic region situated on the conductor adjacent to the corner, V_c is the electric potential (in volts) of the conductor, and V_s is the electric potential at a point in the medium displaced from the corner's apex along a line through the cube's diagonal and at a distance equal to that diagonal. Q is the charge on the cube's three surfaces lying along the conductor's surfaces. Such a configuration is convenient for a finite-difference computation of capacitance.**

I. INTRODUCTION

This paper concerns the capacitance coefficients of three-dimensional (3-D) conductors, a matter of importance to microwave transmission networks, VLSI interconnects, power transmission systems, electric equipment, and electrical insulation technology. Much work has been done on the computation of capacitances for two-dimensional (2-D) models of interconnection lines and other conducting bodies, but much less has been accomplished for 3-D models. Extended bibliographies are given in [6], [7]. A major difficulty arises from the singularities in the electrical field at 3-D corners of a conductor. There are also field singularities along the edges of conductors, but their contributions to capacitances are readily determined by Duncan's correction [2], [5], which is based upon an exact 2-D polar expansion of the field. Since no such exact expansion exists in spherical coordinates, there is no exact 3-D analog of the Duncan correction. Instead, we have sought an approximating asymptotic expansion for the electrical field near a 3-D reentrant corner. There is a literature on this subject; see for an extended bibliography in [7]. Much of this work is of a very general nature dealing with a variety of differential equations and a variety of geometries. The paper of Beagles and Whiteman [1] is the most pertinent one for our purposes. By using the results of that work, we have derived a simple formula that takes into account the concentration of charge at any 3-D rectangular corner. This is most easily used in correcting the capacitances obtained from finite-difference computations.

Manuscript received September 29, 1995; revised February 15, 1996. This work was supported by the National Science Foundation under Grants MIP-9200748 and MIP-9423732.

Y. Zhang is with the Brookhaven National Laboratory, Upton, NY 11973-5000 USA.

A. H. Zemanian is with the Department of Electrical Engineering, University at Stony Brook, Stony Brook, NY 11794-2350 USA.

Publisher Item Identifier S 0018-9480(96)03792-1.